Crosslinking Amine-Modified Silica Aerogels with Epoxies: Mechanically Strong Lightweight Porous Materials

Mary Ann B. Meador[†], *Eve F. Fabrizio*[§], *Faysal Ilhan*[§], *Amala Dass*[#], *Guohui Zhang*[#], *Plousia Vassilaras*[‡], *J. Chris Johnston*[†] *and Nicholas Leventis*[*,†]

NASA Glenn Research Center, 21000 Brookpark Rd., Cleveland OH 44135;

University of Missouri-Rolla, Rolla, Missouri 65409; and Ohio Aerospace Institute, 22800 Cedar Point Rd., Cleveland OH 44142

Abstract

The mesoporous surfaces of TMOS-derived silica aerogels have been modified with amines by co-polymerization of TMOS with APTES. The amine sites have become anchors for crosslinking the nanoparticles of the skeletal backbone of the aerogel by attachment of di-, tri- and tetra-functional epoxies. The resulting conformal coatings increase the density of the native aerogels by a factor of 2-3 but the strength of the resulting materials may increase by more than two orders of magnitude. Processing variables such as amount of APTES used to make the gels, the epoxy type and concentration used for crosslinking, as well as the crosslinking temperature and time were varied according to a multivariable design-of-experiments (DOE) model. It was found that while elastic modulus follows a similar trend with density, maximum strength is attained neither at the maximum density nor at the highest concentration of $-NH_2$ groups, suggesting surface saturation effects. Aerogels crosslinked with the tri-functional epoxide always show improved strength compared with aerogels crosslinked with the other two epoxides under identical conditions. Solid ^{13}C NMR studies show residual unreacted epoxides, which condense with one another by heating crosslinked aerogels at 150 °C.

† NASA Glenn Research Center

§ Ohio Aerospace Institute

University of Missouri-Rolla

‡ NASA LERCIP Summer Intern

* Corresponding Author

1. Introduction

Silica aerogels are among the lowest density, lowest thermal conductivity materials known, with many possible aeronautic and space applications, including vehicles, habitats, planetary rovers and space suits. The use of aerogels as thermal insulation, and/or structural materials could lead to significant weight reductions, enabling future space missions. To date the use of silica aerogels has been limited by their extreme fragility.

Just as dispersion of inorganic nanoparticles in polymers have been shown to improve mechanical, thermal and/or electrical properties of other materials,[1] introducing a polymer into the fragile matrix of a silica aerogel may add strength to the overall composite. Furthermore, chemical bonding (both covalent and non-covalent) between a filler and a polymer improves materials compatibility, enhancing certain properties of a polymeric matrix above and beyond what is accomplished by simple doping with the filler.[2,3,4] By analogy, covalently bonding the polymer to the surface of the aerogel particles should have a similar effect.

We have recently demonstrated that templated polymerization of di- and tri-isocyanates on the surface of the nanoparticle building blocks of silica aerogels increases the strength of the materials by a factor of ~300 for a nominal three-fold increase in density.[5] Crosslinking silica aerogels with isocyanates effectively mimics polyurethane chemistry, where a polyfunctional isocyanate reacts with a polyfunctional alcohol to form carbamates (urethanes). In the case of silica aerogels, the role of the functional polyol is played by the hydroxyl groups on the surface of silica. Thus, it was reasoned that if the surface of silica is decorated with other functionality, for example amines, then epoxy chemistry could be utilized, where a polyfunctional glycidyl ether (i.e., a polyfunctional epoxide) would react with the surface of silica playing the role of a polyfunctional amine (the hardener) to form a hard conformal resin.

Herein, we describe a system where an amine functionality is introduced into silica aerogels by co-polymerization and gelation of tetramethoxysilane (TMOS) and aminopropyltriethoxysilane (APTES) in up to 1:1 volume ratios. The resulting gels are treated with di-, tri- or tetra-functional epoxies in various concentrations. The reaction conditions (time and temperature) are varied along with the APTES concentration, and the epoxy type and concentration, using a statistical experimental design strategy to reduce the number of experiments. The resulting crosslinked gels are dried with supercritical carbon dioxide into aerogels, which are characterized macroscopically, microscopically, and chemically. The most distinct property of polymer crosslinked aerogels is the greatly improved mechanical properties compared to native aerogels. Therefore, special emphasis is given to their strength as a function of the chemical composition, processing conditions and resulting density.

2. Experimental

Materials. Tetramethylorthosilicate (TMOS), aminopropyltriethoxysilane (APTES), diglycidylaniline (di-epoxy), *N,N′*-diglycidyl-4-glycidyloxyaniline (tri-epoxy), 4,4′-methylenebis(*N,N′*-diglycidylaniline) (tetra-epoxy) and ammonium hydroxide (ACS reagent grade) were used as received from Aldrich Chemical Company. Solvents used in the production of crosslinked epoxy aerogels included methanol (ACS reagent grade), tetrahydrofuran (THF: ACS reagent grade), anhydrous tetrahydrofuran (ACS reagent grade purified and dried using a solvent purification system by Innovative Technology, Inc.), and acetone (ACS reagent grade). Supercritical drying was performed using liquid carbon dioxide (standard T type tank with a siphon tube, AGA Inc., Cleveland OH).

Statistical Analysis. Experimental design and analysis was carried out using the RS/Series for Windows, including RS/1 Version 6.01, and RS/Discover and RS/Explore Release 4.1, available from Domain Manufacturing Corporation, Burlington, MA.

Methods. *Preparation of wet gels (hydrogels).* All gels were prepared by mixing together two solutions, A and B. Solution A contained a variable volume ratio of TMOS to APTES in methanol; solution B contained an equal amount of methanol, the appropriate amount of water and the gelation catalyst, if necessary. Wet gels without APTES were prepared by using TMOS, deionized water and methanol in the molar ratio of 1:3:8.5; gelation was catalyzed by adding 6 μmol of NH_4OH (30%) for every mol of TMOS. Thus, in a typical procedure solution A contains 4.5 mL of methanol, and 3.85 mL of TMOS. Solution B contains 4.5 mL of methanol, 1.5 mL of water and 40 μL of the NH_4OH solution.

Wet gels with APTES were prepared by replacing 25% or 50% v/v of TMOS in solution A with an equal volume of APTES. Importantly, the base catalyst, NH_4OH, can be eliminated from the preparation procedure when APTES is used, because the amine group of APTES itself serves as the gelation catalyst.[6] In fact, to slow down the APTES-catalyzed gelation process long enough to allow pouring the sol into the appropriate molds, solutions A and B had to be cooled in a dry ice-acetone bath prior to mixing. Immediately after mixing the cold solutions, 3.6 mL of each mixture was poured into cylindrical molds (Wheaton Polypropylene Omni-Vials, Part No. 225402) approximately 1 cm in diameter to form the desired cylindrical monoliths for testing. The molds were covered with parafilm and the gels were allowed to age for 48 h. Subsequently, wet gels were carefully removed from the molds and were washed approximately every 12 h with methanol (20 mL) a total of four times. This is to remove NH_4OH if present, but was done for the sake of consistency for all gels. Wet gels were then washed four more times every 12 h, twice with THF (20 mL) and twice with anhydrous THF (20 mL).

Three different percent volume concentrations for each epoxide in anhydrous THF (15%, 45% and 75% v/v) were used for crosslinking. Because of the high viscosity of the epoxides, dissolution was facilitated with heating at *ca.* 50 °C and vigorous shaking. Once the solutions were homogeneous, the wet gels were placed into the desired epoxy solution (20 mL), gently stirred and allowed to equilibrate for 48 h. Subsequently, and while still in the corresponding epoxide solution, wet gels were placed in an oven and allowed to react at specified temperatures (50 °C, 72.5 °C or 95 °C) and length of times (16 h, 44 h or 72 h) as predetermined by a statistical experimental design procedure. Afterwards, crosslinked gels were allowed to cool to room temperature and each gel was first washed four times with anhydrous THF (20 mL each time) in 12 h intervals to remove the unreacted epoxide, and then four times with acetone (20 mL each time). After the final acetone wash, monoliths were transferred together with the final acetone wash solution into an autoclave (SPI-DRY Jumbo Supercritical Point Drier, SPI Supplies, Inc., West Chester, PA) and were dried from supercritical CO_2 (40°C and ~100 bar).[7]

Characterization of surface crosslinked epoxide aerogels. Chemical characterization of epoxy crosslinked aerogel monoliths was conducted by infrared, ^{13}C-NMR and ^{29}Si-NMR spectroscopy. The dry aerogel samples were ground by ball-milling for 5 min using a SPEX 5300 Mixer Mill (SPEX Inc., Edison, NJ). Solid samples were mixed with KBr, pressed into a pellet, and infrared spectra obtained with a Nicolet-FTIR Spectrometer Model 750. Solid ^{13}C-NMR and ^{29}Si-NMR spectra were obtained on a Bruker Avance 300 Spectrometer, using cross-polarization and magic-angle spinning at 7 kHz. The acquisition also employed spinning-sideband suppression using a CPSELTICS sequence. The solid ^{13}C spectra were externally referenced to the carbonyl of glycine (176.1 ppm relative to tetramethylsilane, TMS). The solid ^{29}Si spectra were externally referenced to the silicon peak of the sodium sodium salt of 3-trimethylsilylpropionic acid (0 ppm).

Physical characterization of native and crosslinked silica aerogel samples was conducted by thermogravimetric analysis (TGA), scanning electron microscopy (SEM), and nitrogen-adsorption porosimetry. TGA was performed using a TA Instruments Model 2950 HiRes instrument. Samples were run at a temperature ramp rate of 10 °C min^{-1} under nitrogen or air. Samples for SEM were coated with gold and microscopy was conducted with a Hitachi S-4700 field-emission microscope. For nitrogen-adsorption porosimetry, samples were outgassed at 80 °C for 24 h under vacuum and studies were conducted with an ASAP 2000 Surface Area/Pore Distribution analyzer (Micromeritics Instrument Corp.).

Three-point flexural bending tests were performed according to ASTM D790, Procedure A (Flexural Properties of Unreinforced and Reinforced Plastics and Electrical Insulating Materials), using an Instron 4469 universal testing machine frame with a 2 kN load cell (Instron part number 2525-818) and a three-point bend fixture, with 0.9 in. span and 25 mm roller diameter (Instron part number 2810-182). Typical samples were cylindrical, ~1 cm in diameter and ~4 cm in length. The crosshead speed was set at 0.04 in min^{-1}. Three samples were tested for each composition and the average of the three values are presented in Table 1.

Dielectric characterization was conducted by measuring the capacitance of thin (~9 mm diameter, ~1 mm thick) disks. The thin discs were cut from cylindrical monoliths with a diamond wafer blade (Hudson, Cleveland, OH) and saw (Isomet 11-1180, Low Speed Saw, Buehler Ltd., Evanston, IL). The lateral area of each disc was masked with duct tape and the top and bottom surfaces were sputter-coated with gold using a Baltek MED 20 Sputtering System. Copper wires were Scotch™-taped on the two surfaces, and were connected to an MFJ-259B SWR/RF analyzer (MFJ Enterprises, Inc., Mississippi State, MS), running in capacitance-measurement mode. Capacitance measurements were made at three different frequencies (72, 117 and 174 MHz). The average capacitance values were corrected for fringe-field errors.[8] The

relative dielectric constant ε_r of each sample was calculated using the corrected capacitance, area, and thickness of the samples. The accuracy of the dielectric constant measurements was checked by measuring the dielectric constant of a known material, Plexiglas. The measured value was 2.2 ± 0.2, while the reported value is 2.55 ± 0.13.[9]

3. Results and Discussion

3.1 Preparation of epoxy crosslinked aerogels

The first class of mechanically strong silica aerogels we reported relies on conformally coating the silica nanoparticles of the skeletal framework of the aerogel with a polymer derived from diisocyanates, which bind to silica through reaction with its surface hydroxyl groups.[5] The remaining free isocyanate is hydrolyzed by the water adsorbed on the surface of silica producing an amine that reacts further with more diisocyanate from the solution, filling the mesopores. This process builds tethers (*ca.* pentamers) between skeletal nanoparticles.

Analogous to crosslinking silica aerogels with isocyanates inspired by polyurethane chemistry, we turned to the epoxy chemistry that involves reaction of a diamine with a diepoxide.[10] This approach would require a surface of silica rich with amines that will react with a polyfunctional epoxide introduced in the mesopores. It is known that amine functionalized glass can be obtained by treatment with APTES.[11] A similar approach would also work well for our purposes, but post-treatment of silica hydrogels with APTES unnecessarily introduces several time-consuming wash steps. Alternatively, it is known that owing to the slower hydrolysis of APTES relative to TMOS, including APTES in the sol together with TMOS leads to a regular silica backbone, which is surface-modified with the APTES amines.[6,12] This became the favored approach, but the main challenge was the autocatalytic role of APTES (owing to the base properties of the amine functionality), which, in combination with the high concentrations used in this study, causes instantaneous room temperature gelation upon mixing of solutions A and B

(see Scheme 1). It was found, however, that cooling the two solutions retards gelation long enough to allow time for pouring the sol in the appropriate molds. Once the amine-functionalized gels have been formed, they are exposed to a polyfunctional epoxide leading eventually to a strong lightweight material analogous to their isocyanate-crosslinked counterparts. Scheme 1 summarizes the preparation procedure of the epoxy-crosslinked silica aerogels.

For comparison purposes, previously published protocols were followed for as long as possible in the process. It is noted, however, that although in the case of crosslinked aerogels several of the processing steps could become significantly shorter or eliminated altogether, no such effort was made at this stage. This study is rather focused on the relationship between the crosslinking chemistry with the properties of the resulting aerogels. Therefore, the factors explored in crosslinking amine-modified silica with polyfunctional epoxides are: the amine concentration on the silica backbone, the chemical identity and concentration of the epoxide in the mesopores, and finally the reaction temperature and time. Due to the poor general solubility of the epoxides in methanol, THF was used as the solvent. (In this context, it is noted again that several wash steps could be eliminated, shortening the process of Scheme 1 significantly, if methanol is replaced by THF as the gelation solvent.)

The amine concentration on the silica backbone was controlled by the relative ratio of APTES to TMOS in the sol. Thus the APTES concentration, *a*, was evaluated from 0% up to 50% v/v in the total volume of TMOS+APTES. Higher concentrations of APTES do not produce stable gels. For example, using a 3:1 v/v ratio of APTES to TMOS (75% APTES) produces opaque white, gelatinous (as opposed to rigid) and extremely fragile wet gels, while 100% substitution of APTES for TMOS results in sols that fail to gel altogether. As mentioned above, hydrolysis of APTES is a much slower process than hydrolysis of TMOS; thus one

explanation for the gelatinous texture at 3:1 v/v ratio of APTES to TMOS (75% APTES) could be the fact that the amount of TMOS is too small to form stable gels. However, control experiments show that by keeping the relative ratio of APTES/TMOS to 1:3 v/v while reducing the total amount of APTES+TMOS in the sol, produces gels even when the total amount of APTES+TMOS is reduced by 20 times. Presumably, high concentrations of APTES in the sol may also result in steric interferences to gelation. Hence, while it was deemed reasonable that higher concentrations of APTES might yield the most sites for reaction with an epoxide, lower concentrations of APTES might produce a stronger silica framework to build upon.

Three different epoxy crosslinkers were considered: diglycidylaniline, a difunctional epoxide; *N,N*-diglycidyl-4-glycidyloxyaniline, a trifunctional epoxide; and 4,4′-methylene-bis(*N,N*-diglycidylaniline), a tetrafunctional epoxide. For simplicity, these monomers will henceforth be referred to as di-epoxy, tri-epoxy and tetra-epoxy, respectively, and for

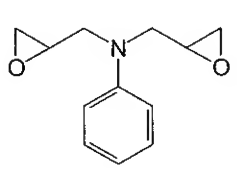

di-epoxy

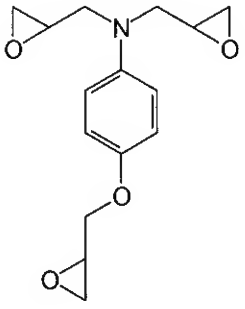

tri-epoxy

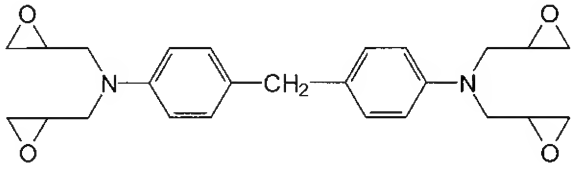

tetra-epoxy

statistical modeling purposes they are represented by the discrete variable, epoxy type, *e*. It is expected that more epoxy groups per molecule might lead to more extensive crosslinking between neighboring amine sites on the skeletal framework. However, it is also deemed reasonable that as the number of epoxy groups increases the molecules might become too constrained for any incremental benefit from the additional reactive sites. By the same token, if

the concentration of the epoxide in the mesopores is too high, then it is expected that single point attachment would occur even when there are no structural constraints for multiple attachment of the epoxide on the skeletal framework.

Thus the effect of the chemical identity of the epoxide on the aerogel properties should be studied in parallel to its concentration, c, in the THF bath. That concentration was varied from 15% to 75% v/v of the corresponding epoxide to THF. Finally, the reaction time, t, and the reaction temperature, θ, which, at first approximation, both control the rate of incorporation of the epoxide into the silica backbone should also be investigated: for one thing, higher temperatures could possibly reduce the epoxide incorporation time, making the process more efficient. Temperature is constrained, however, to a range between ~50 °C, below which the reaction is found empirically to be extremely slow, and ~95 °C, above which we experience excessive solvent boil-off. Thus, it was thought that the inability to increase the reaction temperature indefinitely could be compensated with longer reaction times. The reaction time was varied from 16 to 72 hours.

3.2 Physical properties of epoxy croslinked aerogels

Typical epoxy crosslinked aerogels are shown in **Figure 1**, along with a sample prepared with a 25% APTES to APTES+TMOS volume ratio and no epoxy crosslink (sample furthest to the left). In general, epoxy crosslinked aerogels are translucent. The yellowish coloration observed with uncrosslinked samples is carried over to crosslinked samples as well, and comes from a trace amount of base-catalyzed polymerization of acetone, the solvent that is used in the final washes before supercritical fluid drying.[7] For NH_4OH catalyzed gels, this coloration is avoided by removing the base with alcohol washes before introducing acetone.[7] For APTES

containing gels, this is obviously not possible because the base is an integral part of the gel backbone.

Microscopically, native APTES/TMOS containing gels are similar to typical base-catalyzed gels produced from TMOS. According to the micrograph shown in **Figure 2a,** it is possible to distinguish primary particles clustered together to form larger secondary particles, which in turn form a "pearl-necklace" type of structure with large voids (mesopores). Primary particles leave channels between them leading to the micropores. The epoxy crosslinked samples look similar to one another, irrespective to the chemical identity of the epoxide employed in this study (**Figures 2b-d**). The accumulated material follows the surfaces of the particles conformally, and erases all fine particle definition. In contrast, the mesoporous network survives the process and remains visible in all three crosslinked aerogel samples.

The effect of polymer accumulation on the particles has been quantified as a function of the processing parameters, a, e, c, t and θ as described above using a statistical experimental design approach, by following aerogel properties such as physical dimensions, density, surface area, porosity, strength, and flexibility. It was deemed reasonable to assume that linear and non-linear effects of any variable on any physical property could be captured adequately by a full quadratic model of the form:

$$\begin{aligned} \textit{physical property} = {} & A + B\,a + C\,e + D\,c + E\,t + F\,\theta + G\,a^2 + H\,c^2 + I\,t^2 + J\,\theta^2 + \\ & K\,a\,e + L\,a\,c + M\,a\,t + N\,a\,t + O\,e\,c + P\,e\,\theta + Q\,e\,t + R\,c\,\theta + S\,c\,t + T\,t\,\theta \end{aligned} \qquad (1)$$

where A through T are coefficients that would be derived empirically from experimental data. The model contains terms for first order effects of all five variables and second order terms for a, c, t and θ, as well as all possible two-way interaction terms. (Owing to the discrete nature of variable epoxy type, e, there is no physical meaning to a second order term, e^2.) To evaluate first

and second order terms for a, c, t and θ, a minimum of three levels of each variable must be considered. The three levels of variable a were 0 %, 25 % and 50 % v/v APTES in TMOS+APTES. The three levels of variable c were 15 %, 45 % and 75 % v/v epoxy in THF+epoxy. Variable t was evaluated at 16, 44 and 72 h, and variable θ at 50, 72.5 and 90 °C. The discrete variable epoxy type, e, was also considered at three levels corresponding to the di-, tri- and tetra-functional epoxies discussed.

A full-factorial design to evaluate this model would contain at least 243 experiments (3^5 experiments representing three levels each of five variables), not counting repeats. To minimize the number of experiments, however, a d-optimal experimental design strategy was used.[13] To evaluate the desired model efficiently according to this type of nonclassical design, a set of experimental runs is computer-generated from the 243 candidate experiments.[14] In total, only thirty-three aerogel samples were needed, including 5 repeats to assess model reliability and accuracy. These were prepared according to Scheme 1 in random order, and were analyzed for their physical dimensions, density, surface area, porosity, strength, and flexibility. Table 1 summarizes the design runs and the experimental results.

The density of the samples was determined from their physical dimensions and their weight. Surface area and pore diameters were determined by nitrogen adsorption porosimetry. Mechanical strength data (i.e., stress at break point and elastic modulus) were obtained by a three point bend test method. Density and mechanical strength data for all samples are plotted in **Figure 3** vs. the run order, and distinguished by epoxy type. Since samples were prepared and tested in random order, such time-series plots should and do display a random distribution of values, indicating that no time-dependent errors (e.g., aging of monomers, temperature drift, etc.) are present. For comparison, dotted lines in the graphs show typical values for density, stress at breakpoint and modulus for native aerogels (i.e., non APTES and non epoxy-modified). *Even*

without further analysis, these plots dramatically show that while the density of epoxy-crosslinked aerogels is at most 2-3 times higher than the density of native silica aerogels, both stress at breakpoint and modulus increase by as much as two orders of magnitude. In addition, these plots illustrate that the increases in all three properties is most striking for the tri-functional epoxy.

More systematically, values for selected measured responses (density, surface area, average pore diameter, stress at rupture, and modulus) were analyzed using linear least squares regression of eq 1. All continuous, independent variables were orthogonalized (transformed to the -1 to 1 range) prior to modeling to minimize correlation among terms. Terms not statistically significant (<90% confidence) were dropped from the model one at a time by the stepwise modeling technique. Summary statistics and significant terms in the models are shown in Table 2. Three-dimensional plots of response surface models show the responses graphed vs. only two variables at a time. Effectively, a fourth dimension is included in each graph by showing the three surfaces corresponding to each multifunctional epoxy used in the study. Furthermore, since these are all five-variable models, the two remaining parameters must be held constant in each of the plots. And, since increasing strength has been the primary motivation for this study, graphs of all of the response surface models are presented with the constant variables set at the optimum conditions for strength (*vide infra*). At last, it should be mentioned that in addition to discerning significant relationships between variables and responses, the derived response surface models can also be used to predict the conditions that produce optimum values for the responses.

Selected response surface models for density are shown in **Figure 4**. Density is a commonly cited property of aerogels, and is used to express the fact that they are lightweight materials. Here, we also wish to use density as a measure of the amount of organic matter incorporated in silica. Strictly speaking, because changes in density may also be due to changes

in sample dimension (i.e., shrinkage, expansion), density is not a direct measure of how much epoxide has been attached onto the aerogel framework. However, there is no correlation between density and the physical dimensions of the samples[15] while there is a clear correlation between density and mass loss by TGA analysis,[16] in this case density does comprise a reliable gauge for the epoxide uptake.

Figure 4a-b both clearly show that when the tri-functional epoxy is used more material is incorporated into the aerogel. This is taken as indicative of the difference in reactivity between the epoxide linked through an oxygen vs. those linked through nitrogen to the center aromatic core. If the reactivity of these two kinds of epoxides were the same, then a larger molecule such as tetra-epoxy would have shown higher density increases, especially at lower APTES concentrations where amine sites might be too far apart to allow multiple epoxy moities to bridge across two amines effectively.

More specifically, **Figure 4a** shows the synergistic effect on density between the number of reactive amine sites (percent APTES) and the epoxy concentration. At 0% APTES, increasing epoxy concentration in the THF bath has little effect on the density (since reactivity of any epoxide with the –OH groups on the surfaces of a native aerogel is expected to be low), while at higher concentrations of APTES, increasing the epoxy concentration from 15 to 75% causes the density to double. It is curious that density reaches a maximum at around 30% APTES, above which it levels off. This would seem to suggest that at higher concentrations of APTES, as the surfaces of the aerogel particles become fairly crowded with amine sites, more epoxy molecules begin to bridge multiple amine sites, but after a certain APTES concentration, amine sites remain unreacted. **Figure 4b**, which shows density graphed vs. time and temperature, illustrates that these variables have only a slight effect on density when epoxy and APTES concentration are

held at their optimum conditions for strength. At lower concentrations of APTES, both have a more pronounced effect on density.[17]

Nitrogen adsorption data were analyzed for average pore sizes and surface areas by the Brunauer-Emmet-Teller (BET) method. A selected response surface for surface area is shown in **Figure 5a**. In general, by comparing the BET surface area shown in **Figure 5a** with that for density in **Figure 4a**, we conclude that samples with the higher density have lower surface area. The tri-epoxy samples, which have the highest densities are the lowest in surface area, followed by tetra and di-epoxy samples. Surface area decreases with increasing epoxy concentration, APTES concentration, time and temperature, while density increases under the same conditions. This inverse relationship between surface area and density has been observed before with isocyanate crosslinkers,[5] and was attributed to the fact that accumulated crosslinker clogs channels to the micropores, making those surfaces inaccessible for nitrogen adsorption.[18] What is interesting, however, is that a comparison between the BET surface area of epoxy and isocyanate crosslinked samples of similar densities reveals that epoxy samples show significantly higher surface areas. For example, tri-epoxy crosslinked samples with densities in the range of 0.4-0.5 g/cm^3 have surface areas in the range of 278-443 m^2/g. Isocyanate crosslinked samples with densities in the same range have surface areas in the range of 277-165 m^2/g. This observation implies that epoxy crosslinked samples are substantially more porous, presumably permitting access to some micropores. This in turn should be related to the structure of the crosslinker, which consists of long chains in the case of isocyanates, but mostly short chain linkages in the case of epoxies (see Section 3.3 below).

Finally, the surface area models for di-epoxy and tetra-epoxy shown in **Figure 5a** are almost exactly on top of one another, whereas the density models in **Figure 4a** show much higher densities for the tetra-epoxy samples than the di-epoxy ones. This is presumably because

the tetra-epoxy weighs twice as much as the di-epoxy. At similar epoxy incorporation—expected since the reactivities of the di-epoxy and the tetra-epoxy should be the same—density increases more with the tetra-epoxy, while surface area does not change as much.

Figure 5b shows response surfaces plotted for average pore diameter with fixed variables held constant at the optimum strength as previously described. Surprisingly, the general trend in the pore diameter models of **Figure 5b** is somewhat different from what is observed for the BET surface area and the density. One would expect that as more material accumulates on the nanoparticles, more microchannels would become clogged preventing access to micropores thus shifting the average pore size to larger dimensions. Hence, di-epoxy crosslinked aerogels with the lowest density and largest surface areas would be expected to exhibit the smallest pore diameters, and those made with tri-epoxy, having the highest density and the smallest surface areas, would be expected to exhibit the largest pore diameters. In fact, the tetra-epoxy samples exhibit the smallest pore diameters while the di-epoxy samples have the largest pore diameters under almost all processing conditions. Clearly, the parameters affecting pore diameter are more complex then can be explained by merely greater incorporation of material. Tri-epoxy crosslinked aerogels appear to be the least sensitive to changes in APTES and epoxy concentration, exhibiting a nearly flat response across the design space.

Stresses at breakpoint and moduli for the aerogel samples were calculated from stress-strain curves obtained from three point bend test results similar to those shown in **Figure 6** for two randomly selected samples of variable density. The experimental conditions and data analysis were identical to those applied for isocyanates and have been described in detail before.[5] Much like with isocyanate crosslinked aerogels, stronger samples are also stiffer (they require a higher force for a given amount of deformation) and tougher (larger area underneath the stress-strain curve; i.e.; they can store more energy at the breakpoint). The most characteristic

difference from isocyanate crosslinked aerogels is the almost completely elastic behavior of epoxide crosslinked aerogels (as demonstrate by the linear stress-strain relationship) all the way to the point of rupture.[5] Again, this is probably attributed to the fact that polymer is actually built up in the case of the isocyanate crosslinked aerogels but not in the case of epoxies (refer to Section 3.3).

For modeling purposes, maximum stresses at breakpoint were first normalized by the log transform. The maximum predicted value for stress is 2.28×10^6 N/m^2 (predicted for a = 29.2% APTES, e = tri-epoxy, c = 54.2% v/v tri-epoxy in the THF bath, θ = 50 °C and t = 72 h). Monoliths made under these conditions are predicted to have a density of 0.497 g cm^{-3}, pore diameter of 146.1 Å, surface area of 351.7 m^{2}g^{-1} and a modulus of 133.12 MPa. Similarly, modulus was also normalized by a log transform before modeling. The maximum predicted value for modulus is 220 MPa (predicted for a = 33.6 % APTES, e = tri-epoxy, c = 75% v/v tri-epoxy in the THF bath, θ = 50 °C and t = 72 h). Monoliths made under these conditions are predicted to have a density of 0.583 g/cm^3 and a stress at rupture of 2.04 MPa.

Selected response surface models for stress at rupture are shown in **Figure 7a** with processing time and temperature held constant at optimum conditions for stress at break (72 h and 50 °C, respectively) and in **Figure 7b** with APTES and epoxy concentration held constant also at optimum conditions for maximum stress at rupture (29.2% APTES and 54.2% v/v epoxide in the THF bath, respectively). Thus, **Figure 7a** illustrates the pronounced second order effect of APTES concentration on the maximum stress similar to that for density, but unlike density, stress reaches a clear maximum for epoxy concentration in the THF bath at approximately 50%. Apparently, incorporation of more epoxy beyond that point, as evidenced by the further increase in density, does not contribute any additional strength. Presumably, this is

because at epoxy concentrations in the THF bath of ~50% v/v, crosslinking between amine functionalities reaches a maximum. Beyond that point more epoxy may be incorporated but does not lead to crosslinking as it may remain attached to only one amine group. In turn, **Figure 7b** shows the significant synergistic effect between reaction time and temperature. At higher temperatures, increased reaction time does not result in increased strength, while at lower temperatures there is a clear increase in strength over the time studied. Indeed, the graph suggests that reacting longer then 72 h may lead to a further increase in strength.

Response surface models for modulus are shown in **Figure 8**. In **Figure 8a** we notice a very similar trend as with density, but with a more pronounced maximum at approximately 33% APTES concentration. Additionally, at the optimum APTES concentration, modulus does not level off at a lower optimum epoxy concentration as does maximum stress, but continues to increase over the entire range studied, reaching a maximum at 75% epoxy. In the same context it is also noted that there is a similar correlation of the modulus with density between the epoxy crosslinked aerogels of this study and isocyanate crosslinked aerogels from our previous work.[19] These results are taken to signify that unlike strength, crosslinking is most probabaly not a prerequisite for higher modulus. In other words, the aerogel modulus can be increased further by incorporation of material on the silica nanoparticles whether it is crosslinked or not. **Figure 8b** again shows a very pronounced interaction between time and temperature at the optimum levels for epoxy and APTES concentrations. The highest modulus is obtained with reaction temperature and time at the lowest and longest values respectively, but nearly equal results can be obtained using the shortest time and the highest temperature.

At this point it is evident that incorporation of epoxy increases strength over and above what is expected by simple densification, while relatively large surface areas and not much larger pore diameters imply that mesoporosity has been retained. Therefore, it is reasonable to expect

that reinforcement of silica aerogels through crosslinking should not affect the properties that render aerogels attractive materials for practical applications. One such application, which has not been realized owing to the usual fragility associated with native aerogels, is as a dielectric material. Since aerogels consist mostly of empty space, they are expected to have relative dielectric constants close to that of air (ε_{air}=1) rendering them ideal insulators for fast electronics. Dielectric constants of samples close to the optimum strength were determined by measuring the capacitance across discs cut from larger monolithic pieces similar to those used for measuring strength. Capacitance values were corrected for fringe-field effects and the relative dielectric constants, ε_r, were calculated from the corrected capacitance, and the physical dimensions of the discs (area and thickness) as described in detail before.[5d] Table 3 summarizes the results. The values are in the same range as those measured and reported with isocyanate crosslinked samples of similar densities, and significantly lower than the dielectric constants of dense silica (~4.2),[20] or of typical epoxies (~3.5).[21] The low relative dielectric constants confirm that as far as practical applications are concerned, crosslinking leaves the mesoporous void space mostly unaffected.

3.3 Chemical characterization of crosslinked aerogels

Both increases in density as well as strength clearly show that all samples treated with epoxies have incorporated material leading to mechanically strong samples. Infrared spectroscopy[22] is of limited value in assessing the chemical identity of the epoxy reinforced aerogels. Although there are distinct features in both the 1600-1500 cm^{-1} and the 800-700 cm^{-1} range associated with the incorporated epoxy, nevertheless, the presence of the broad O-Si-O vibration band in the 1100-1000 cm^{-1} region prevents determination of whether some epoxy groups (expected in the 1250-1150 cm^{-1} range) remain unreacted under the conditions of the experimental design. Thus, we turned to NMR spectroscopy to monitor chemical changes to

silica aerogels incorporating APTES and epoxy. Incorporation of APTES into the aerogel structure can be followed by ^{29}Si and ^{13}C CP-MAS NMR. **Figure 9a** shows the ^{29}Si CP-MAS spectrum of aerogel prepared from TMOS alone. The three peaks in the spectrum can be assigned to silanediol (-90.6 ppm), silanol (-99 ppm) and siloxane (-108.8 ppm) as previously reported by Maciel et al.[23, 24]

Figure 9b shows the ^{29}Si CP-MAS spectrum of an aerogel with 25% APTES incorporated into the matrix. The peaks at -90.6 and -99 ppm are greatly reduced. The new peak at -65.1 ppm corresponds to tridentate bonding (three Si-O bonds) of the APTES silicon to the silica matrix.[25] There is only a slight distortion on the left side of this broad peak that could correspond to a very small amount of mono or bidentate bonding peaks which fall in the region of -50 to -54 ppm. There does not appear to be any reaction of silica with the APTES amine, which has been shown to occur in the gas phase at high temperatures. Those silicons would appear around -25 ppm.[25] **Figure 9c** shows the spectrum for an aerogel prepared with 50% APTES incorporated, which is nearly identical to **Figure 9b** except that the silicon from APTES at -65 ppm is about doubled in size and the hump on the low-field side of the peak corresponding to mono or bidentate silicon bonding is a little more pronounced.

As shown in **Figure 10a**, ^{13}C CP-MAS NMR of 50% APTES containing aerogels have three main peaks (10.5, 24.8 and 44.1 ppm) assigned to the three carbons of the APTES propyl group. Resonances at 15 and 50 ppm are assigned to a small amount of residual ethoxy groups from APTES and the small peak at 164 ppm is due to a small amount of imine from the surface amines reacting with acetone, used to wash these samples before supercritical drying. In the epoxy crosslinked aerogels, acetone was not used until after epoxy incorporation (refer to Scheme 1). The absence of imine peak in these samples indicates that at least the amines available on the surface are all consumed by reaction with epoxy before the final acetone washes.

The reaction between the glycidyl ether groups of the epoxies with the surface amines of APTES is expected to occur through simple addition as shown in Scheme 2.[26] In the absence of catalysts and higher temperatures, extensive homopolymerization is not expected to occur.[27] Intramolecular etherification (cyclization) becomes a significant product with the amine-linked glycidyl groups at 150 °C especially at low concentration of amine. Reactions were monitored by C^{13} CP-MAS NMR as shown for a select number of samples from the experimental design. In all of the spectra, the presence of the epoxides can be observed by their distinct aromatic signature, as well as the aliphatic peaks at approximately 45 to 75 ppm representing both reacted and unreacted epoxy moieties. Although at much diminished relative intensity, two of the aliphatic carbons of the aminopropyl group of APTES are still observable at 10.5 and 24.8 ppm. The APTES peak for carbon at the α-position relative to the nitrogen, which should be shifted to the 50-55 ppm region after reaction with the epoxide, is hidden under the epoxy resonances.

The spectra of typical di-epoxy crosslinked aerogels, shown in **Figures 10b** and **10c**, has four aromatic peaks corresponding to the carbon bonded to nitrogen (148.5 ppm), the carbons meta to nitrogen (128.7 ppm), para to nitrogen (115.3 ppm) and ortho to nitrogen (112.08 ppm). The spectrum in **Figure 10b**, which corresponds to sample No. 21 made using no APTES and a much more concentrated epoxy solution (75% v/v in the THF bath) shows a significant amount of unreacted epoxy rings (51.8 ppm) along with a peak at 71.2 ppm which can be assigned to epoxy reacted with siloxy groups.

It should be emphasized that although we are able to detect reaction between the epoxides and the aerogel surface in the absence of APTES, much more crosslinking occurs when APTES is present, as expected.[28] This is obvious by comparing the densities of samples prepared with and without APTES; for example, sample No. 9, made using 50% APTES concentration and only 15% v/v of the di-epoxy in the THF bath, whose spectrum is shown in **Figure 10c,** has a

30% higher density and three times the strength of sample No. 21 (made using no APTES). In the aliphatic region of **Figure 10c**, a broad resonance from 55 to 67 ppm can be assigned to amine-reacted epoxide. Unreacted di-epoxy has three aliphatic carbons which have peaks at 44.7, 49.9 and 52.5 ppm.[29] In solid NMR, this shows up as one broad peak at ~52 ppm. As expected, because the sample is made from the highest amount of APTES and the least concentrated epoxy solution, there are very few unopened epoxy rings in this sample, since this distinct resonance at ~52 ppm is not present.

Typical spectra of the tetra-epoxy cross linked aerogels, shown in **Figures 11a** and **11b**, have three aromatic peaks corresponding to carbon bearing the nitrogen at 146.8 ppm, meta to nitrogen at 129.7 ppm, and ortho to nitrogen at 112.4 ppm. In the aliphatic region of **Figure 11a**, which represents reaction of 75% epoxy with an aerogel containing 0% APTES from sample No. 3, there is a small amount of reacted epoxide (broad resonance from 60-72 ppm) and a much sharper peak (51.0 ppm) for unreacted epoxides. Most likely, one out of the four epoxide rings is reacting with the silica aerogel, leaving the other three unreacted. The sharp peak at 29.5 ppm is likely due to residual solvent (acetone) in the aerogel. **Figure 11b** shows the spectrum of tetra-epoxy crosslinked aerogel made with 50% APTES and 15% epoxy (sample No. 19). The broad resonance at 50-69 ppm probably reflects an approximately equimolar mixture of reacted and unreacted epoxy rings indicating that some bridging of neighboring APTES sites is occuring. The resonance at 43.7 ppm can be assigned to the carbon α– to the amine in unreacted APTES.

Typical spectra for the tri-epoxy are shown in **Figures 12a-c**. Each spectrum has three aromatic peaks assigned to phenoxy carbon at 151.1 ppm, carbon with nitrogen attached at 143.2 ppm and the unsubstituted carbons at 115.0 ppm. **Figure 12a** shows the spectrum of sample No. 12, which was made with no APTES and 45% tri-epoxy concentration. The aliphatic region contains broad peaks at 45 and 51 ppm that can be assigned to the carbons of unreacted epoxy

rings as well as a resonance at 70 ppm, belonging to carbons from epoxy which has reacted with siloxy. There appears to be about a 2:1 ratio between reacted to unreacted epoxy present in the sample, suggesting that on the average two out of the three epoxy moieties in each tri-epoxy molecule have reacted creating a bridge between neighboring APTES sites. **Figure 12b** shows the spectrum of sample No. 27, prepared with 25% APTES and 45% tri-epoxy concentration; a similar 2:1 ratio between reacted and unreacted epoxy moieties is apparent, though the strength and density for this sample is much higher than the sample prepared without APTES. **Figure 12c** shows sample No. 20 made with 50% APTES and 45% tri-epoxy concentration. Here, the unreacted epoxy peaks appear to be approximately the same size as the amine-reacted epoxy peaks, indicating that some of the tri-epoxy is linked to only one APTES group.

These observations indicate that at best two epoxy groups per molecule react with the aerogel suface (whether APTES or siloxy group), regardless of whether there are two, three or four epoxy moieties available per molecule. Furthermore, a higher percentage of APTES in the aerogel does not necessarily provide more cross linking between APTES sites. Rather, more epoxy is bonded to only one APTES, especially evident in the case of the tri-epoxy when the maximum amount of APTES is used. This is consistent with the maximum stress model which shows that the best strength is obtained for medium values of APTES and epoxy, with higher APTES concentrations providing increased density aerogels with no further increase in strength.

As mentioned previously, since homopolymerization or intermolecular cyclization of epoxy become significant modes of cure for epoxies at higher temperatures, it was anticipated that post-curing the monoliths at 150 °C could force unreacted epoxides dangling from the mesoporous surfaces of the aerogels to crosslink further as shown in **Scheme 2**. This is indeed the case. Several samples of the tri-epoxy crosslinked aerogels from the design were subjected to post-curing by heating in vacuum for five hours at 150 °C. A representative solid ^{13}C NMR of

post-cured epoxy crosslinked aerogel (sample run 27) is shown in **Figure 13.** Compared to the spectrum of the as-processed sample 27 shown in **Figure 12b,** the very pronounced peaks at 45 and 51 ppm belonging to unreacted epoxy groups have all but disappeared. Only a broad lump at 55-57 ppm remains, which is assigned to the aliphatic carbons attached to nitrogen in the fully reacted epoxy. As shown in Table 4, the epoxy crosslinked aerogels shrink only about 5% after exposure to the 150 °C post-cure as evidenced by the change in diameter of the samples. This shrinkage is directly related to the amount of epoxy present in the samples as reflected by their density. Sample 12 has the least epoxy because there is no APTES in the sample. The other three samples, 22, 6 and 27 in that order, show an increase in density, and hence with shrinkage, correlated with reaction time. Whether this post-cure treatment leads to a further increase in strength or changes other properties of the monoliths is currently under investigation.

4. Conclusions

We have utilized a statistical experimental design approach to identify the reaction conditions to produce epoxy crosslinked aerogel monoliths with optimized properties. Thus, we have been able to expand the scope of our methodology of producing mechanically strong aerogels in two ways: (a) we have modified the surface of silica with amines; and (b) we have adopted epoxy chemistry for crosslinking the silica nanoparticles through the amines, producing strong lightweight materials analogous to the isocyanate crosslinked aerogels previous reported.

Epoxy crosslinked aerogels appear more elastic and retain higher porosity than their isocyanate counterparts. The trifunctional epoxide yielded the strongest crosslinked aerogels mainly due to it's increased reactivity over the bifunctional and tetrafunctional epoxides we employed. Maximum strength is attained neither at the maximum density nor at the highest concentration of $-NH_2$ groups, suggesting surface saturation effects. Therefore, we have

identified a most favorable combination of $-NH_2$ group concentration with optimal exposure to epoxide for maximum crosslinking. Residual unreacted epoxy groups are forced to react with one another by heating dried aerogels at ~150 °C. This post-curing process might provide a means to increase strength further without building up additional weight. Furthermore, it might have important implications for the overall processing of epoxy crosslinked aerogels by, for example, shortening cure time.

Acknowledgments. The authors thank Linda McCorkle of the Ohio Aerospace Institute for the SEM images, Daniel A. Scheiman of QSS Group for running thermal analysis, Emily Berkeley for running some of the solid NMR and Anna Palczer for porosimetry measurements. We are also grateful to the NASA Glenn IR&D Program for the support of this work.

Supporting Information Available. Appendix I: Plot of experimental runs from the D-optimal experimental design. Appendix II: Plot of sample density versus monolith diameter. Appendix III: A typical TGA plot and a graph of sample density vs. overall weight loss by TGA. Appendix IV: Response Surface Models for weight loss by TGA. Appendix V: Dependence of density on reaction time and temperature at low concentrations of APTES. Appendix VI: Comparison of strength at rupture and modulus vs. density of epoxy and isocyanate crosslinked silica aerogels. Appendix VII: Infrared spectra of typical APTES-modified, epoxy crosslinked silica aerogels.

Table 1. Design of Experiments and Physical Characterization for the Resulting Epoxy Crosslinked Silica Aerogels

Run	APTES percent	Epoxy type	Epoxy percent	Time, h	Temp, °C	Density, g/cm^2	Surface Area,[c] m^2/g	Average Pore Diam.,[d] Å	Load force, kg	Max Stress, 10^5 N/m^2	Modulus, MPa	Weight loss, %
1	50	tetra	75	16.00	50.0	0.42	358	105	2.318	3.70	44.07	62
2	25	tri	15	44.00	72.5	0.42	443	116	5.112	7.78	53.50	66
3	0	tetra	15	72.00	95.0	0.44	662	125	2.497	3.46	33.33	58
4	50	di	75	16.00	95.0	0.30	462	114	0.990	1.33	13.30	60
5	25	tri	45	44.00	72.5	0.48	350	134	5.820	8.77	72.64	64
6	25	tri	45	44.00	72.5	0.47	355	151	6.942	10.12	71.95	63
7	25	tri	45	44.00	95.0	0.51	280[e]	143[f]	11.448	16.93	87.93	68
8	50	di	75	72.00	50.0	0.32	446	186	0.978	1.39	18.84	57
9	50	di	15	72.00	95.0	0.30	439	180	0.965	1.32	11.56	57
10	25	tri	45	44.00	72.5	0.49	328	146	9.439	14.16	82.17	63
11	25	tri	75	44.00	72.5	0.59	290	120	5.275	8.88	126.29	64
12	0	tri	45	44.00	72.5	0.36	267	140	2.225	2.97	18.28	54
13	0	tetra	75	72.00	50.0	0.24	670[e]	83[f]	a	a	a	14
14	50	di	15	16.00	50.0	0.28	493	86	0.661	0.96	14.55	47
15	25	tri	45	44.00	72.5	0.49	309	141	5.473	8.04	74.67	63
16	25	tetra	45	44.00	72.5	0.42	450	125	3.196	4.95	46.50	55
17	0	tetra	15	16.00	50.0	0.20	821	112	a	a	a	10
18	25	tri	45	44.00	72.5	0.48	343	147	7.269	10.99	78.69	62
19	50	tetra	15	16.00	95.0	0.32	464	132	1.466	2.00	17.66	59
20	50	tri	45	44.00	72.5	0.40	278	91	5.750	7.47	34.98	70
21	0	di	75	72.00	95.0	0.24	444	100	0.341	0.45	3.24	32
22	25	tri	45	16.00	72.5	0.44	345	156	5.155	7.44	63.17	60
23	50	tetra	75	72.00	95.0	0.41	335[e]	104[f]	2.195	3.15	32.99	66
24	50	tetra	15	72.00	50.0	0.32	459	99	1.521	2.18	19.43	56
25	0	di	15	16.00	95.0	0.26	784	175	a	a	a	13
26	25	tri	45	44.00	72.5	0.47	312	151	7.775	11.28	71.46	63
27	25	tri	45	72.00	72.5	0.49	314	147	12.950	19.05	80.08	64
28	25	tri	45	44.00	50.0	0.47	316[e]	119[f]	6.043	9.39	70.41	60
29	0	di	15	72.00	50.0	0.21	856	62	a	a	a	10
30	25	di	45	44.00	72.5	0.33	546	145	1.855	2.79	24.35	45
31	0	tetra	75	16.00	95.0	0.29	423	115	0.440	0.67	6.94	28
32	28	tri	35	72.00	50.0	0.45	b	b	7.21	10.03	52.00	b
33	29	tri	35	72.00	50.0	0.48	b	b	7.39	11.57	50.70	b

[a] Samples were too fragile for testing.

[b] Samples not-tested.

[c] Surface area of non-crosslinked aerogels: 25% APTES=739 m^2/g; 50% APTES=622m^2/g.

[d] Pore diameter of non-crosslinked aerogels: 25% APTES=117 Å; 50% APTES=89 Å.

Table 2. Significant terms and summary statistics for response surface models.

Response	Significant terms	R^2	Standard (RMS) error
Density	a, c, e, t, θ a^2, c^2 $a*t, a*\theta, a*c, e*c, e*t, t*\theta, a*e$	0.999	0.0066 g/cm^2
BET Surface Area	a, c, e, t, θ a^2, c^2 $a*\theta, a*c, e*c, e*\theta, t*\theta, a*e$	0.988	26.54 m^2/g
Average Pore Diameter	a, e, t, θ a^2, t^2, c^2 $a*t, e*c, e*\theta, a*e$	0.962	7.75 Å
Stress at rupture (log transformed)	a, c, e, t, θ a^2, c^2 $a*t, a*\theta, a*c, e*c, t*\theta$	0.985	1.197 N/m^2
Modulus (log transformed)	a, c, e, t, θ a^2, c^2 $a*t, a*\theta, a*c, e*c, t*\theta, e*t$	0.998	1.006 MPa

Table 3. Dielectric constants, ε_r, for APTES-modified silica aerogel monoliths reacted with di-tri- and tetra-functional epoxides.

Sample No.	Epoxy type	Density, g/cm^3	ε_r
1	tetra	0.42	1.80
2	tri	0.42	1.80
5	tri	0.48	1.90
6	tri	0.47	2.30
7	tri	0.51	1.90
9	di	0.30	1.70
10	tri	0.49	2.40
11	tri	0.59	2.50
12	tri	0.36	2.00
15	tri	0.49	2.30
16	tetra	0.42	2.10
18	tri	0.48	2.20
20	tri	0.40	1.90
22	tri	0.44	2.20
23	tetra	0.41	2.20
24	tetra	0.32	2.10
26	tri	0.47	1.90
27	tri	0.49	2.10
28	tri	0.47	2.20

Table 4. Sample diameters and percent shrinkage for aerogels post-cured at 150 °C. (All samples were originally made from 45% tri-epoxy at 72.5 °C.)

Sample No.	APTES, percent	Time, h	Density, g/cm^3	Sample diameter, cm		Shrinkage, percent
			before	before	after	
12	0	44	0.36	0.976	0.934	4.3
22	25	16	0.44	0.877	0.838	4.5
6	25	44	0.47	0.906	0.862	4.9
27	25	72	0.49	0.898	0.850	5.4

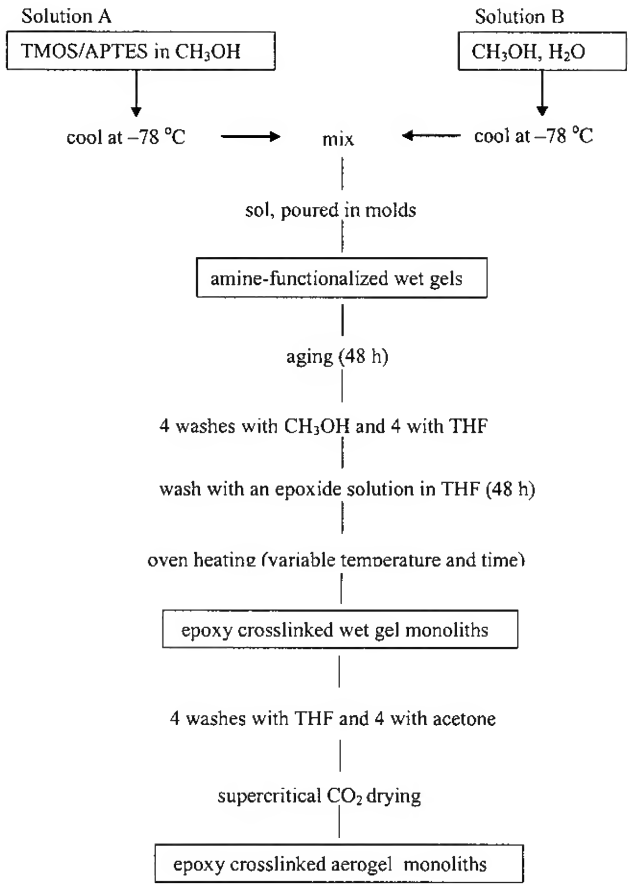

Scheme 1. Flowchart for the Preparation of Epoxy Crosslinked Aerogels

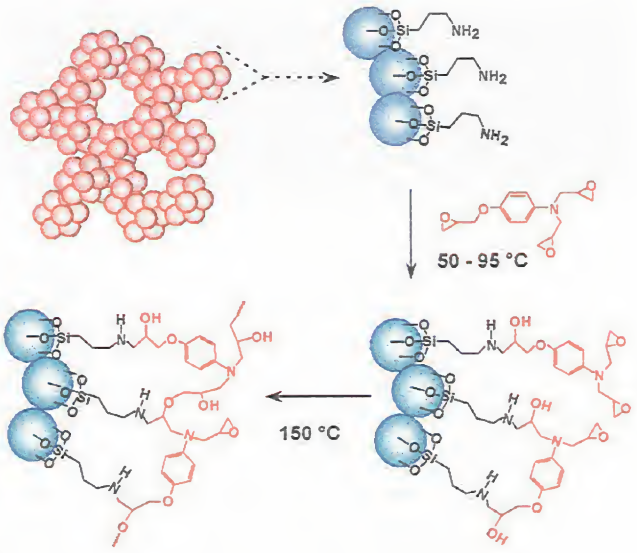

Scheme 2. Reaction of tri-epoxy with surface amines on APTES modified aerogels.

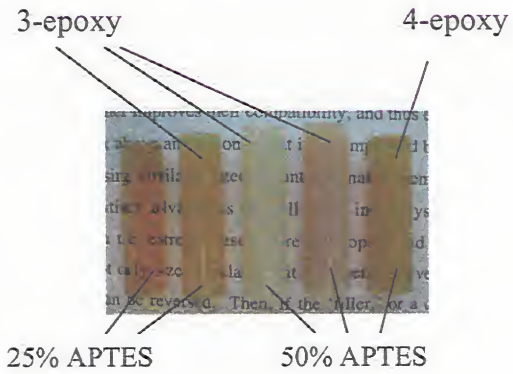

Figure 1. Photograph of representative samples of APTES-modified, epoxy crosslinked aerogels.

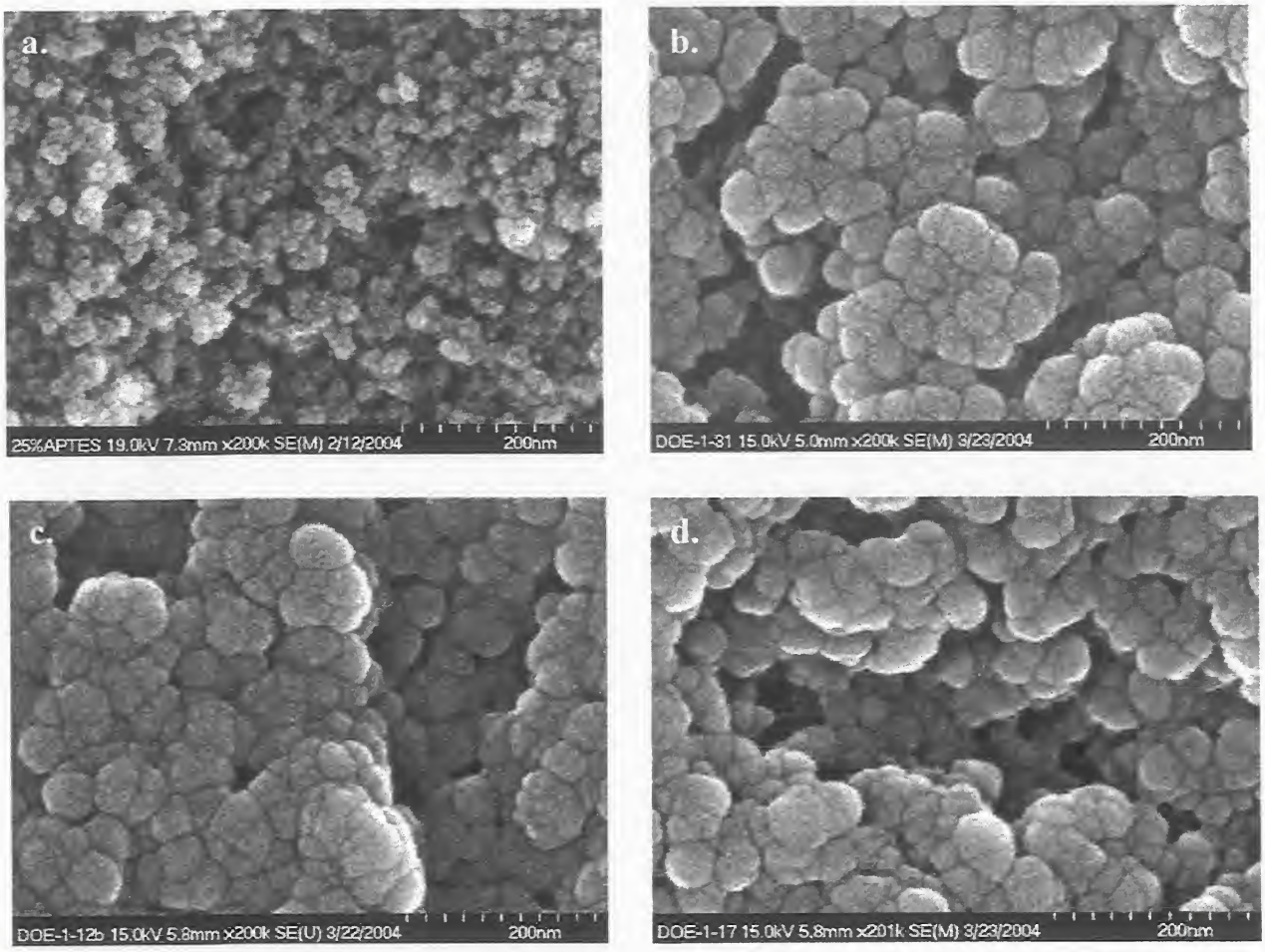

Figure 2. Scanning Electron Microscopy of a) 25% APTES without epoxy, b) 25% APTES with di-epoxy (run 30), c) 25% APTES with tri-epoxy (run 11), and d) 25% APTES with tetra-epoxy (run 16).

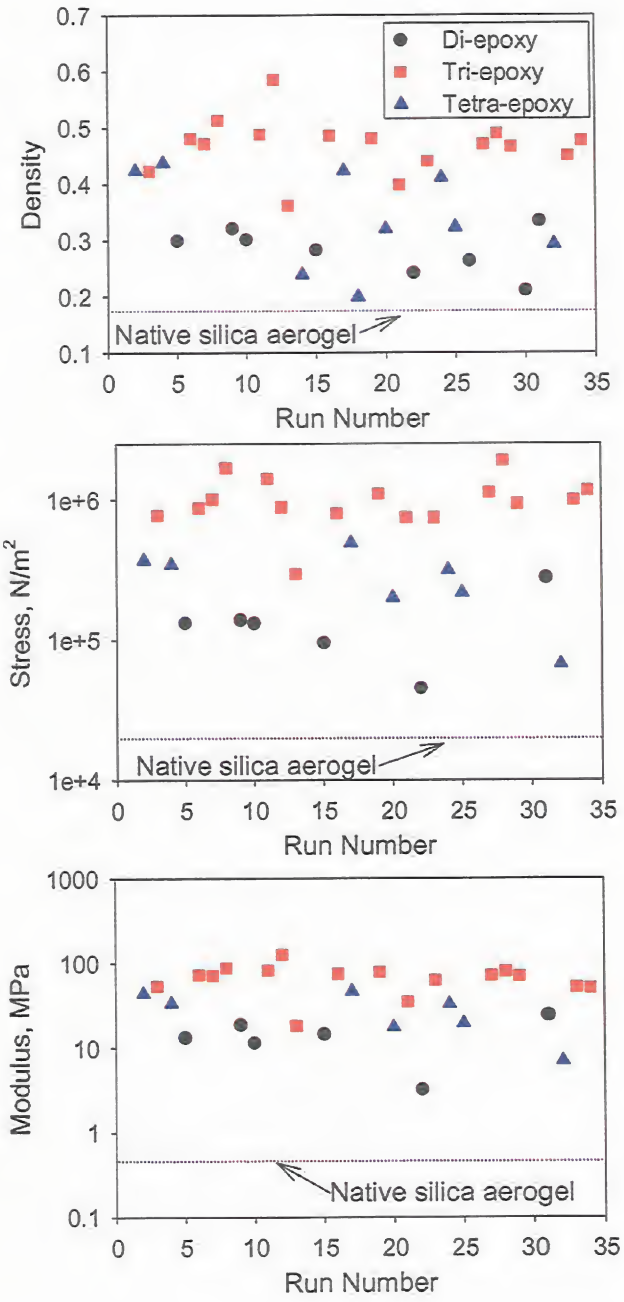

Figure 3. Time series plots of runs from the experimental design compared to native silica aerogels made using TMOS (no APTES—see experimental section).

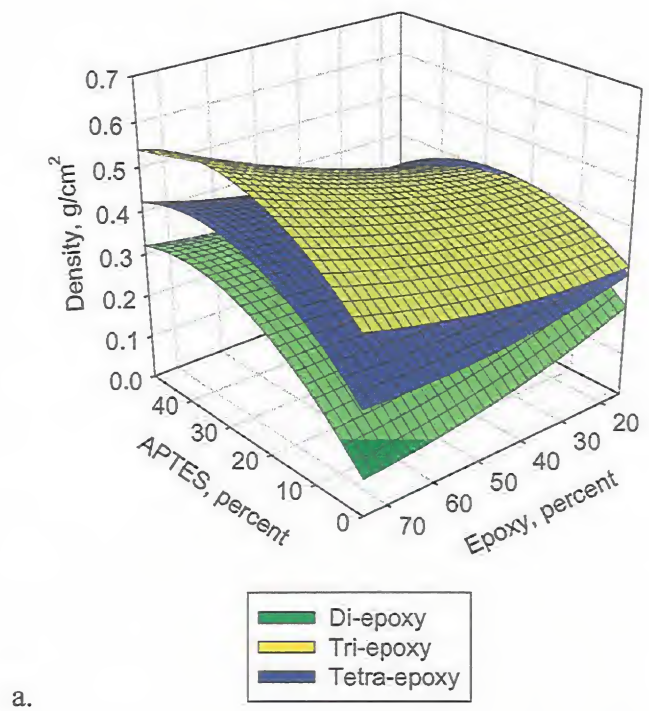

a.

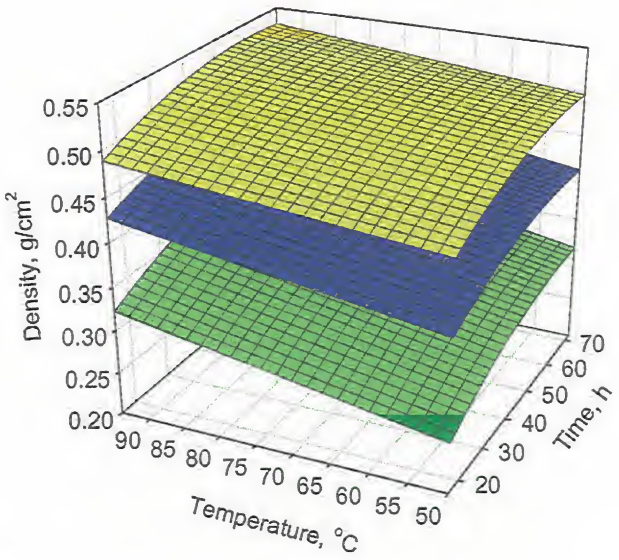

b.

Figure 4. Response surface models for density graphed *versus* a) APTES and epoxy concentration with time and temperature held constant at the predicted optimum values for stress, and b) time and temperature with epoxy and APTES concentration held constant at the predicted optimum values for stress.

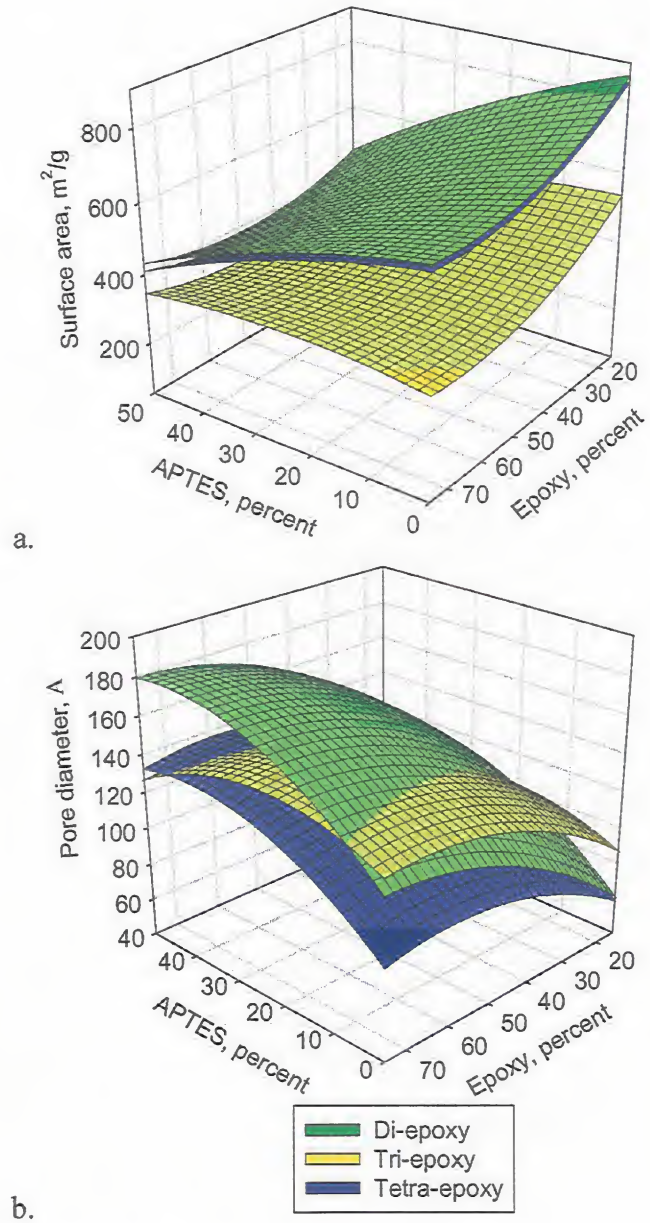

Figure 5. Response surface models for a) BET surface area and b) pore diameter graphed *vs.* APTES and epoxy concentration with time and temperature held constant at the predicted optimum values for stress.

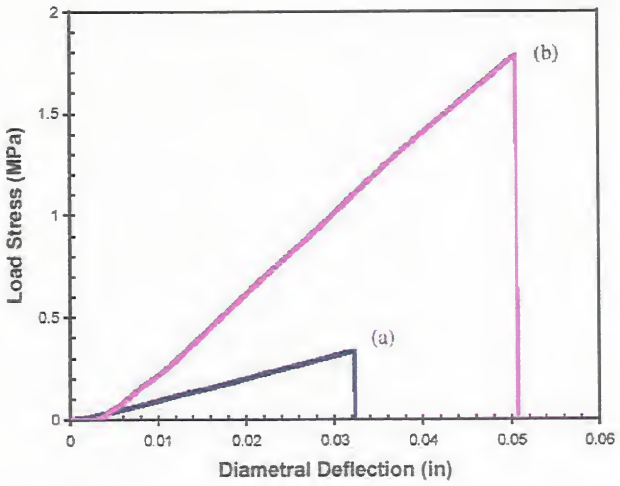

Figure 6. Stress strain curves of samples from a) run 23 (using tetra-epoxy) and b) run 7 (using tri-epoxy).

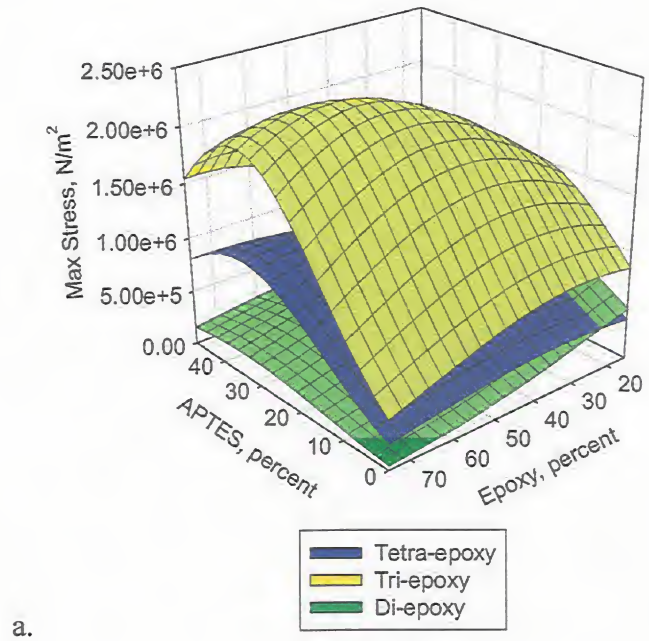

a.

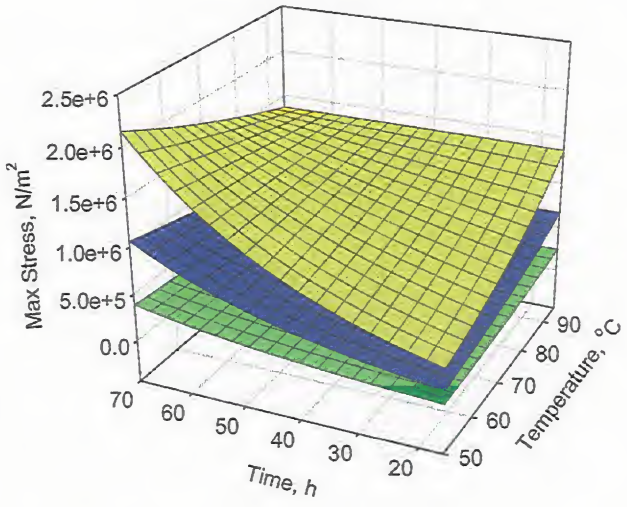

b.

Figure 7. Response surface models for maximum stress at rupture graphed *vs.* a) APTES and epoxy concentration with time and temperature held constant at the predicted optimum values for stress, and b) time and temperature with epoxy and APTES concentration held constant at the predicted optimum values for stress.

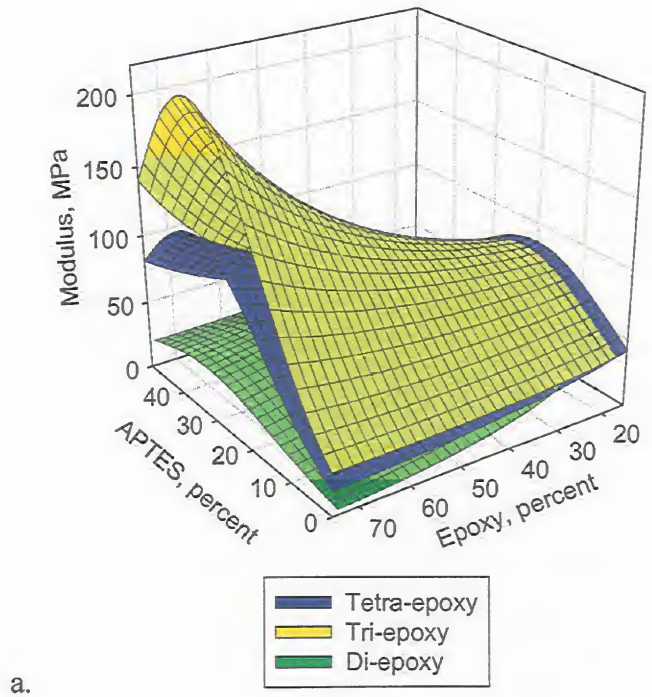

a.

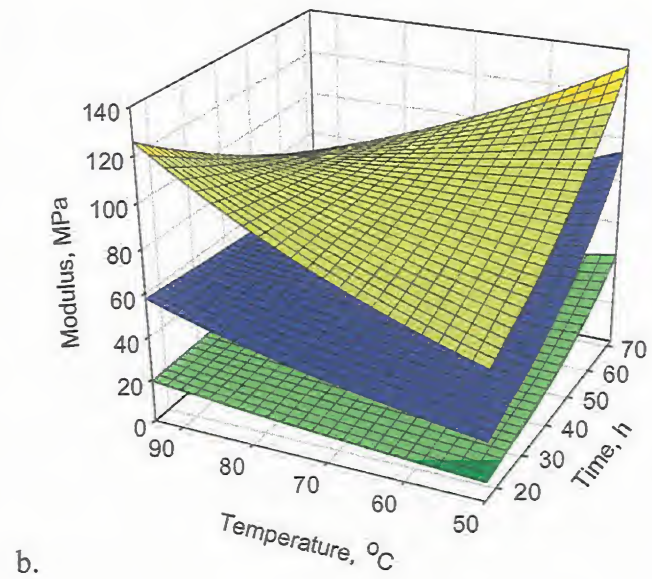

b.

Figure 8. Response surface models for modulus graphed *vs.* a) APTES and epoxy concentration with time and temperature held constant at the predicted optimum values for stress, and b) time and temperature with epoxy and APTES concentration held constant at the predicted optimum values for stress.

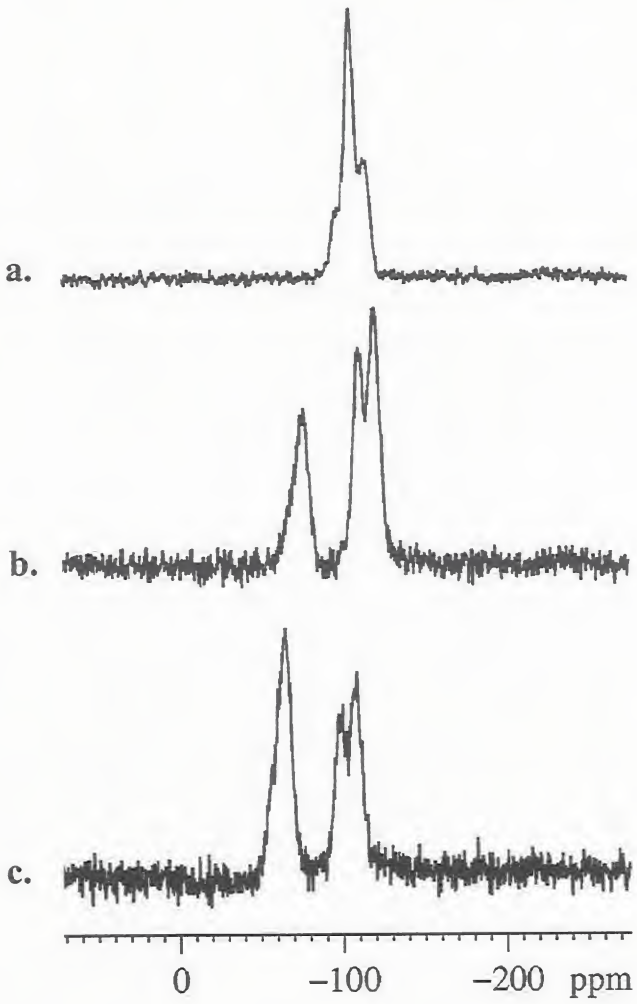

Figure 9. ^{29}Si CPMAS NMR of aerogel made with TMOS and a) 0% APTES, b) 25% APTES and c) 50% APTES.

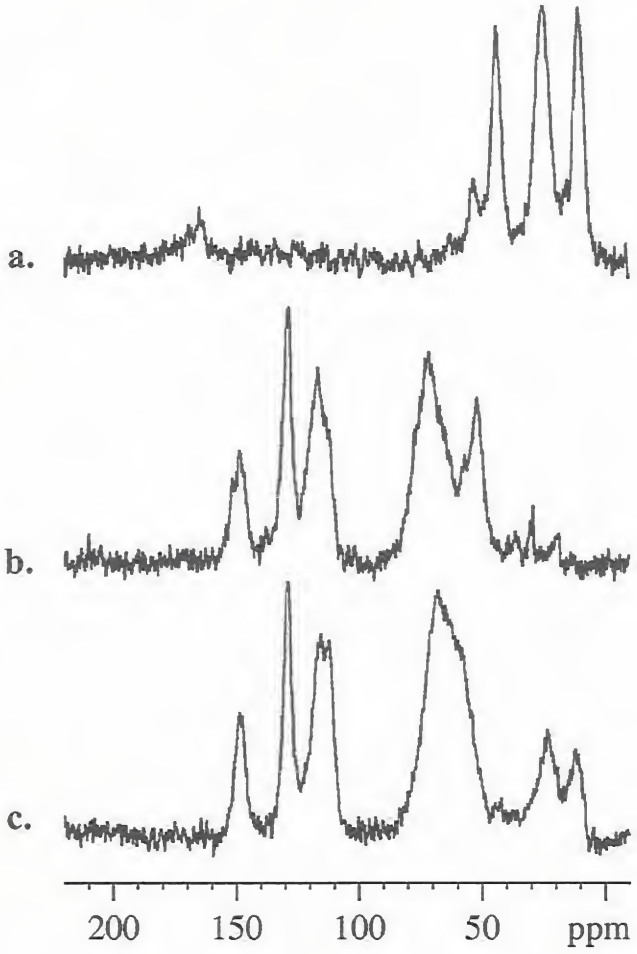

Figure 10. ^{13}C-NMR of a) 50% APTES; b) no APTES with di-epoxy (run 21); c)50% APTES with di-epoxy (run 9).

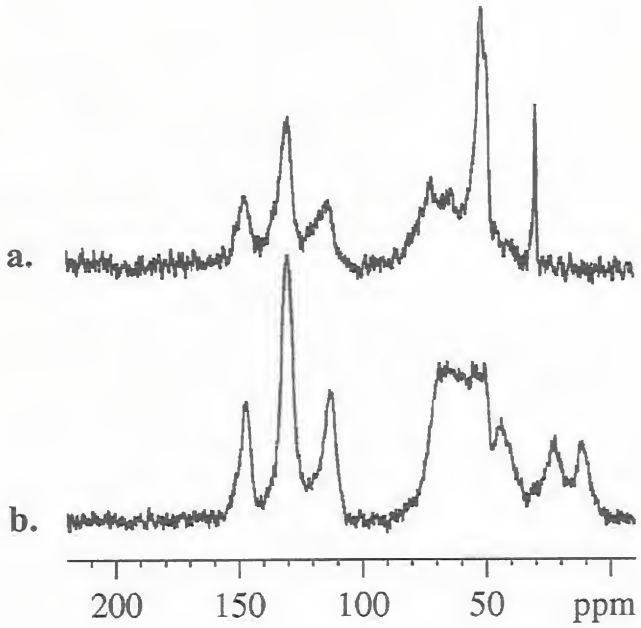

Figure 11. ^{13}C-NMR of a) no APTES with tetra-epoxy (run 3); b) 50% APTES with tetra-epoxy (run 19).

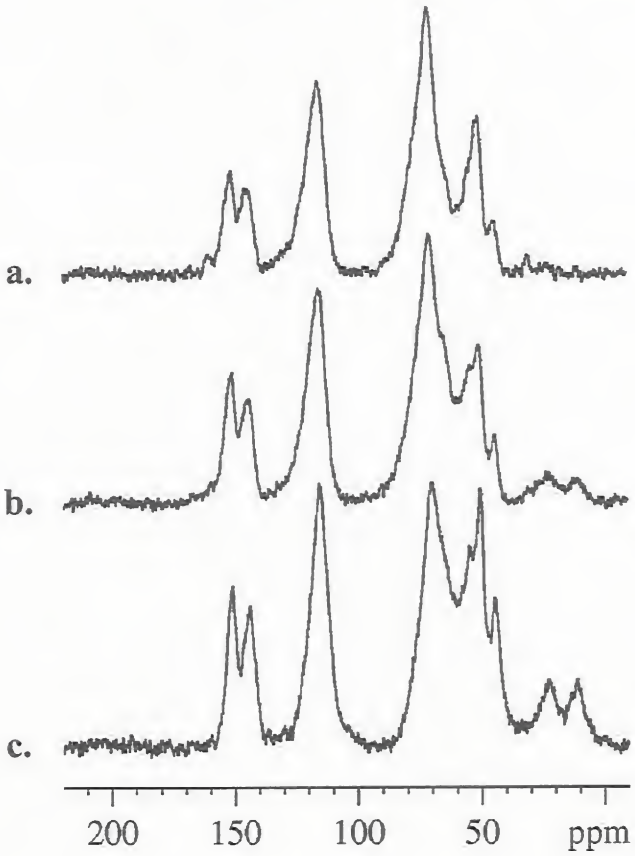

Figure 12. ^{13}C-NMR of a) no APTES with tri-epoxy (run 12); b) 25% APTES with tri-epoxy (run 27); c) 50% APTES with tri-epoxy (run 20).

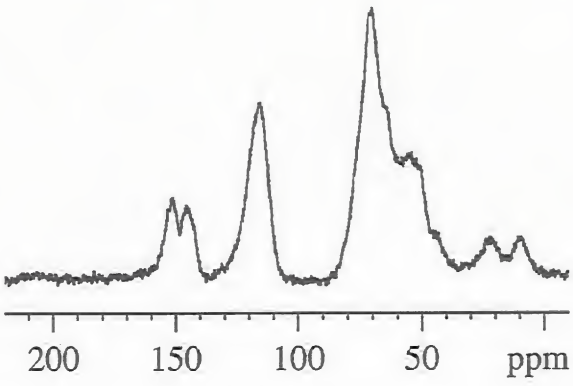

Figure 13. ^{13}C-NMR of sample from run 27 (25% APTES with tri-epoxy) after 5 hour post-cure at 150 °C.

References

1. Thayer, A. M. in *Chemical & Engineering News*, September 1, 2003 issue, p. 15.

2. (a) Chen, Y.; Iroh, J. O. *Chem. Mater.* **1999**, *11*, 1218-1222. (b) Ahmad, Z.; Mark, J. E. *Chem. Mater.* **2001**, *13*, 3320-3330.

3. Campbell, S.; Scheiman, D. *High Performance Polymers* **2002**, *14*, 17-30.

4 . Mitchell, C. A.; Bahr, J. L.; Arepalli, S.; Tour, J. M.; Krishnamoorti, R. *Macromolecules* **2002**, *35*, 8825-8830.

5 . (a) Leventis, N.; Sotiriou-Leventis, C.; Zhang, G.; Rawashdeh, A.-M. M. *Nano Lett.* **2002**, *2*, 957-960. (b) Zhang, G.; Rawashdeh, A.-M. M.; Sotiriou-Leventis, C.; Leventis, N. *Polymer Preprints* **2003**, *44*, 35-36. (c) Bertino, M. F.; Hund, J. F.; Zhang, G.; Sotiriou-Leventis, C.; Tokuhiro, A. T.; Leventis, N. *J. Sol-Gel Sci. Tech.* **2004**, *30*, 43-48. (d) Zhang, G.; Dass, A.; Rawashdeh, A.-M. M.; Thomas, J.; Counsil, J. A.; Sotiriou-Leventis, C.; Fabrizio, E. F.; Ilhan, F.; Vassilaras, P.; Scheiman, D. A.; McCorkle, L.; Palczer, A.; Johnston, J. C.; Meador, M. A.; Leventis, N. *J. Non-Cryst. Solids* **2004**, *350* 152-164.

6. Hüsing, N.; Schubert, U.; Mezei, R.; Fratzl, P.; Riegel, B.; Kiefer, W.; Kohler, D.; Mader, W. *Chem. Mater.* **1999**, *11*, 451-457.

7. Leventis, N.; Elder, I. A.; Rolison, D. R.; Anderson, M. L.; Merzbacher, C. *Chem. Mater.* **1999**, *11*, 2837-2845.

8. Sloggett, G. J.; Barton, N. G.; Spencer, S. J. *J. Phys. A: Math. Gen.* **1986**, *19*, 2725.

9. Reza, A. *IEEE Trans. Microwave Theor. Techn.* **1998**, *46*, 1307.

10. Billmeyer, Jr., F. W. *Textbook of Polymer Science, 3rd Edition*, John Wiley and Sons; New York: New York, 1984, p 31.

11. (a) Nemeth, S.; Yin, R.; Ottenbrite, R. M.; Siddiqui, J. A. *Polymer Preprints* **1997**, *38*, 365-366. (b) Chiang, T. H.; Nakamura, A.; Toda, F. *Thin Solid Films* **1989**, *182*, L13-L16.

12. Hüsing, N.; Schubert, U. *Angew. Chem. Int. Ed.* **1998**, *37*, 22-45.

13. For a description of D-optimal and other statistical experimental design strategies, see Montegomery, D. C. *Design and Analysis of Experiments*, **1997**, John Wiley and Sons, Inc., Hoboken, NJ and references therein.

14. Further discussion of how the runs were derived is described in Appendix I in Supporting Information.

15. See Appendix II in Supporting Information.

16. See Appendices III and IV in Supporting Information.

17. See Appendix V in Supporting Information.

18. A possible source of error with BET analysis of organic surfaces is chemisorption (as opposed to physisorption) of nitrogen, evidenced by non-super positioning of the adsorption/desorption isotherms. Since the desorption part of every isotherm retraced the foot of its adsorption part, we conclude that there is no chemisorption problem. Indeed, according to BET theory, typical values of C are between 5 to well over 100. Values <5 indicate that gas to gas affinity is competing with gas to solid making BET assumptions unworkable. Values much greater than 100, indicate very strong attraction of the gas for the surface or preferential adsorption. If the surface area is above 500 m^2/g, and particularly if C is above

300, results should be questioned. In our case surface areas are well below 500 m^2/g and all C-values fall between 48 and 80, confirming that none of these potential problems are present.

19. See Appendix VI, Supporting Information.

20. Maex, K.; Baklanov, M. R.; Shamiryan, D.; Iacopi, F.; Brongersma, S. H.; Yanovitskaya, Z. S. *J. Appl. Phys.* **2003**, *93*, 8793-9941.

21. See for example: Chen, W.-Y.; Wang, Y.-Z.; Kuo, S.-W.; Huang, C-F.; Tung, P.-H.; Chang, F.-C. *Polymer* **2004**, *45*, 6897-6908.

22. See Appendix VII, Supporting Information.

23. Maciel, G. E.; Sindorf, D. W. *J. Am. Chem. Soc.*, **1980**, *102*, 7606-7607.

24. It should be noted that cross polarization enhances the peaks for silicons in closest proximity to the hydroxy or alkoxy protons (-90.6 and -99 ppm peaks) more than those further away (-108.8 ppm). Hence, in an NMR spectrum run without cross polarization (not shown), the siloxane peak is slightly larger then the silanol peak and the silanediol appears only as a slight hump on the left side of the central silanol resonance. This more accurately represents the ratio between the different silicon species.

25. Ek, S.; Iiskola, E. I.; Niinisto, L.; Vaittienen, J.; Pakkanen, T. T.; Root, A. *J. Phys. Chem. B*, **2004**, *108(31)*, 11454-11463.

26. Matejka, L.; Dusek, K. *Macromolecules* **1989**, *22*, 2902-2910.

27. Matejka, L. *Macromolecules* **2000**, *33*, 3611-3619.

28. Davis, S. R.; Brough, A. R.; Atkinson, A. *J. Non-crystalline Solids* **2003**, *315*, 197-205.

29. Poranski, C. F.; Moniz, W. B. *J. Coatings Technology*, **1977**, *49(632)*, 57-61.